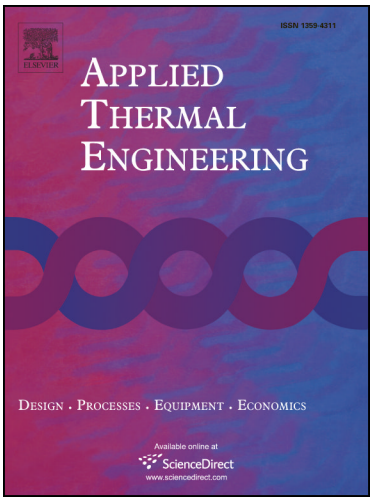

Research Paper

Applicability of CSP solar fields to the dry cooling of related thermodynamic cycles

H. Espargilliere, L. del Campo, P. Echegut, X. Py, M. Muselli, D. Rochier

PII: S1359-4311(17)30616-6
DOI: http://dx.doi.org/10.1016/j.applthermaleng.2017.08.028
Reference: ATE 10910

To appear in: *Applied Thermal Engineering*

Received Date: 27 January 2017
Revised Date: 29 June 2017
Accepted Date: 5 August 2017

Please cite this article as: H. Espargilliere, L. del Campo, P. Echegut, X. Py, M. Muselli, D. Rochier, Applicability of CSP solar fields to the dry cooling of related thermodynamic cycles, *Applied Thermal Engineering* (2017), doi: http://dx.doi.org/10.1016/j.applthermaleng.2017.08.028

Applicability of CSP solar fields to the dry cooling of related thermodynamic cycles

H. Espargilliere[a], L. del Campo[b], P. Echegut[b], X. Py[a,*], M. Muselli[c], D. Rochier[d]

[a]*PROMES-CNRS UPR 8521, Processes, Materials and Solar Energy, University of Perpignan Via Domitia, Rambla de la thermodynamique, Tecnosud 66100 - Perpignan cedex, FRANCE.*
[b]*CEMHTI-CNRS UPR 3079, 1D avenue de la Recherche Scientifique, 45071 - Orléans cedex 2, FRANCE.*
[c]*SPE UMR CNRS 6134, University of Corsica, Vignola, Route des Sanguinaires, F-20000 - Ajaccio, FRANCE.*
[d]*EXOSUN SAS, Rue Jacques Monod, Technopole Bordeaux, Montesquieu 33650 - Martillac, FRANCE.*

* Corresponding author : py@univ-perp.fr,Tel.: + 33468682215.

Abstract – Concentrating Solar Power (CSP) technologies in arid areas suffer of a too high water consumption at the condenser of their power-block. The different alternative dry cooling technologies previously proposed to overcome this weakness lead to a decrease of 3 to 7% in whole efficiency of the power plant and a corresponding increase of 10% in the cost of the produced electricity. The new dry cooling approach proposed in the present study is based on using the solar field (SF) as a macro heat exchanger. Nightly, the extended available surface area of the SF allows convective thermal exchange with the surrounding environment and additional radiative heat transfer with the 3K extra atmospheric space through the atmospheric window in between 8-14 µm. The exchanged radiative heat flow density depends directly on the optical properties of the exposed materials. In the present paper, performances of conventional and innovating reflective materials are presented through the assessment of their spectral emissivity. Aluminum film (innovating material) appears to be the most efficient one with a mean spectral emissivity around 95%, while glass mirrors (conventional materials) area round 86%. Moreover, within the spectral range of the atmospheric window 8-14 µm, aluminum film is more stable than the glass mirror with a respective standard deviation of 3 and 7.8 respectively. The results confirm that radiative heat transfer can contribute to the cooling needs of linear Fresnel and parabolic trough CSP plant power block at a level of 95% and 53% respectively.

Keywords – Concentrated Solar Power, water consumption, dry cooling, mix heat transfer, radiative cooling.

Nomenclature

ε_λ	Spectral emissivity
ρ_λ	Spectral reflectivity
τ_λ	Spectral transmission
ε_{spec}	Specular emissivity
ρ_{spec}	Specular reflectivity
ε_{diff}	Diffuse emissivity
ρ_{diff}	Diffuse reflectivity
$L_\lambda(T)$	Spectral radiance (W/(m².sr.µm))
$L_\lambda^0(T)$	Spectral radiance of blackbody (W/(m².sr.µm))
h	Planck constant (m².kg/s)
c	Speed of light (m/s)
λ	Wavelength (µm)
k	Boltzmann constant (m².kg/(s².K))
T	Temperature (K)
$L(T)$	Total spectral radiance (W/(m².sr))
$M(T)$	Radiative flux density (W/m²)
CSP	Concentrated Solar Power
SF	Solar Field
LCA	Life Cycle Analysis
TES	Thermal Energy Storage
IR	Infra Red
GM	Glass Mirror
RFSM	Reflective Film of Silver Mirror
AM	Aluminum Mirror
PVD	Physical Vapor Deposition
FT	Fourier Transform
DTGS	Deuterated Tri-Glycine Sulphate detector
MCT	Mercury Cadmium Telluride
SD	Standard Deviation
SRC	Steam Rankine Cycle

1. Introduction

Recent published worldwide energy demand analysis [1] estimate significant future increase in electricity demand for which renewable energies sources and technologies should be mobilized and developed to contribute to the so-called energy-mix. In this context, concentrating solar power (CSP) is expected to contribute up to 10% to this share in 2050. According to the amount of already implemented plants [2], this would correspond to an average worldwide annual CSP growing of 40%. Thanks to the two last decades, those technologies have already demonstrated their reliability at industrial scale and can be considered as mature. Nevertheless, their extensive growing to achieve the energy transition could simultaneously induce major mineral resources depletions [3] and environmental impacts [4]. In fact, the various components of those CSP technologies have been mainly designed and developed during the eighties whereas the today's environmental constrains and related design tools are drastically different or were even not available. As an illustration, full life cycle analysis (LCA) of CSP plants have been published only recently [5] highlighting major issues related to their sustainability. Among them, while alternative approaches have been recently proposed for the thermal energy storage component [6,7], only few studies address the whole water consumption needed at the condenser of their power block [8-12].

Since the very early SEGS (1985) solar trough plants in USA up to the very recent Gemasolar (2012) or Crescent-Dune (2015) central receiver ones, the power block of all commercial CSP plants (**Fig. 1.a**) already under operation are based on conventional super heated steam thermodynamic cycle (**Fig. 1.b**) such as all regular thermal power stations. The whole efficiency of the power block is directly function of the area of the water/steam cycle and then to the highest temperature offered by the solar field on one side and to the lowest condensing temperature on the other side. The highest temperature level is limited by both the selected concentrating technology and available absorber materials (today roughly 400°C for linear concentration and 800°C for central receiver concentration). As the power block efficiency ranges roughly at 33%, 2 thermal MW of waste heat at about 55°C [12,13] have to be discharged to the surrounding environment for every MW of power produced. Considering that the most suitable implementation sites of CSP plants are arid areas within the so-called solar belt, the temperature of the surrounding environment is drastically too close to the condensing one, especially during the hottest hours of the day. Up to date, the most efficient and current way to overcome this issue is to use water evaporating cooling facilities [14] already acknowledged [2-4] to be responsible of a too high water consumption (3.7 m^3/MWh) with respect to the low water availability in arid area.

Those last decades, the cooling tower technology has benefited from major innovations [15,16] leading to better performances, reduction in water consumption, reduction in investment and O&M costs. Nevertheless, a wet cooling technology still remains inappropriate for a CSP process intended to arid areas. In the particular case of CSP, the available extended surface of the solar field could offer the advantageous possibility to avoid such wet cooling device. Beyond this specific application, the proposed dry radiative

approach could also be further considered for other ones presenting low grade waste heat with no potential valorization.

The alternative dry option [17], already used in few plants such as PE1 (2009, Spain), consists of using air cooled heat exchangers inducing drastically a reduction in the cycle efficiency from 3 to 5% and a parasitic electric consumption of about 7%. A hybrid combination has been also proposed enhancing the cooling power of dry coolers during the hottest hours by complementary water evaporation [18]. Other scarce published studies propose a valorization of the waste heat to drive sea water desalination units [19,20] or other low temperature power systems such as solar chimney [21-23].

The aim of the present work is to contribute to an emerging option very recently proposed in the literature [8-12] identifying the solar field of the CSP plant as a potential macro heat exchanger (**Fig. 2**). According to those preliminary studies, the solar field is a key CSP component in terms of investment (40 to 50% of the initial plant investment [13]) and land occupation (200 ha for a conventional 50 MWe solar trough plant such as ANDASOL 2009 Spain) while it is obviously only used daily. Therefore, it would be rather advantageous and strategic to use this extended available surface for multifunctional purpose and especially as macro heat exchanger.

Preliminary thermal studies [8] and more recent extended simulations [11,12] have already demonstrated the relevance and efficiency of this approach. Roughly, considering the available reflective surfaces of the different CSP solar field and as illustrated in **Fig. 3** and **Table 1**, the waste heat to be discharged per available square meter ranges from 140 to 400 W/m² for an average value of 250 W/m². This range of heat transfer rate can be reasonably achieved by means of the two simultaneous heat transfer mechanisms, namely the convective heat transfer with the surrounding air and the radiative heat transfer with space (a huge available heat sink at 3K) through the atmospheric window (**Fig. 4**). Due to lower surrounding temperature and high radiative efficiency, the cooling potential is higher nightly while the waste heat has to be discharged daily or even 24h/day in case of a CSP plant involving extended high temperature thermal energy storage (TES). This mismatch can be managed by an additional low temperature TES sub unit.

On the heat exchanging surfaces level, two major options have been proposed: one using the back side of the solar field surfaces as radiative exchangers [12], the other one considering the reflective solar surfaces as infrared (IR) radiative exchangers [10]. The advantage of the last one would be to avoid the cost of additional radiative material, to avoid any modification of the reflective surfaces supports and to produce coldness 24h/day. Nevertheless, this approach can be realistic if the solar reflective surfaces used in CSP present good IR radiative properties. Even if numerous studies have been published since the pioneer works of Felix Trombe [24], they are related to various conventional (white paint [25,26], aluminum [27],...) or selective surfaces (TiO_2 coating [28,29],...) but no reflective surface such as mirror to our knowledge. Those studies mostly applied to building cooling [30] and fresh water production by condensation of moisture [31,32] demonstrate rather uniformly a range of cooling rate of 50 to 70 W/m² and a maximum undercooling below the environment temperature down to -

40°C [24]. Therefore, the assessment of IR radiative properties of CSP reflective surfaces, both conventional and innovative, remains highly needed for further consideration of the above dry cooling concept.

The concentrating technology considered in the above mentioned study [10] is the simplest one, namely the Linear Fresnel. It offers as a first step a basic geometry of rather flat rectangular mirrors (see **Fig. 2**) in parallel, each one tracking the sun by rotation on their main longitudinal axis. Practically, this rotational axis is made of a hollow metallic tube on which the mirror's support is fixed (**Fig. 5a**). The most basic configuration of the approach consists to use this tube to distribute the waste heat by flowing a heat transfer fluid through it. A more advanced configuration consists to replace the mirror support by a flat heat exchanger such as the Roll-bond technology (flat on one side and channeled on the other) offering better HTF distribution and higher heat transfer performances (**Fig. 5b**).

In the present paper, conventional glass mirror currently used in CSP (recent and also aged) and emerging technologies such as metallic reflectors or films are characterized and compared in terms of IR radiative properties with respect to the spectral transparency of the atmospheric window.

2. Materials and characterization method

2.1 Investigated materials

The reflective surfaces characterized in the present study were selected among those available in the CSP market. Two type of conventional materialsused as reflectors in CSP plants and new innovative surfaces under development were selected and investigated, they are listed below with their available characteristics :

(1) GM : conventional reflective materials are basically the glass mirrors historically used in the first CSP plants of the 80's such as the Themis solar tower pilot plant and still used in new plants. Glass mirrors (labeled GM in the paper) supplied by the Saint Gobain company (France) were sampled at Themis. They are composed of a silvered layer deposited at the back side of a 6 mm thick glass.

(2) RFSM : innovative thin reflective films of silver mirror manufactured by the 3M company (U.S.) are considered today as light and inexpensive materials of high potential for CSP in the future. The experimented material is the solar mirror film 2020® characterized by a thickness of 127 μm, a superficial weight of 0.263 kg/m², a total solar reflectance (ASTM E903, G173) greater than 93%, a specularity (D&S, 15 mrad, 660 nm) greater than 97% and an operating temperature range from -40°C to 65°C.

(3) AM : aluminum mirrors innovating materials differ from conventional ones by their multi-thin-layered composition. Already used as reflectors in recent CSP prototypes such as the parabolic trough pilot of Microsol [33] developed by the Exosun company (France), they

are usually made of a reflective film of aluminum stuck on aluminum substrate support structures of 2 mm thickness supplied by Almeco and Alucoil. The experimented ones in the present study were namely the Vegaprime-WR193® of Almeco (labeled AM 1) and the Almirr-203® from Alucoil (labeled AM 2).

The experimented AM composite mirrors present a 2 mm thickness obtained by lamination of a plastic resin core (1.4 mm) between two aluminum layers (0.3 mm). The top layer is an anodized aluminum with multilayer coating including a highly reflective weather resistant foil of aluminum 1090 alloy (purity 99.9%) deposited by Physical Vapor Deposition (PVD). The back layer is an aluminum sheet protected by a corrosion resistant coating. The two composite mirrors characterized in the present study (AM 1 and AM 2) differ by their respective multilayer coating composition and the thickness of their top layer.

The top layer of AM 1 is composed by (from bottom to the top): an anodized aluminum substrate, a 99.99% pure aluminum reflective layer, a low optical index reflectance enhancing layer, a high optical index reflectance enhancing layer, a highly transparent hard and resistant against the effects of abrasion and weathering top coat.

Concerning AM 2, its commercial announced specular reflectance is 87.6%. Its top layer is composed by (from bottom to the top): an anodized aluminum substrate (0.3mm thick) which is deposited on the aluminum substrate by Physical Vapor Deposition and subsequently coated with a protective lacquer ceramic for an outdoors use. Its back layer is a polyester paint. These mirrors are currently used in Almeria at the PSA-CIEMAT test facilities.

Those reflective surfaces (RFSM and AM) present several major advantages as compared to conventional glass mirrors. They present lower superficial weight (5 and 10 times less respectively) and higher stiffness (about 10 times more) leading to easier handling, transport and implementation. The structure also allows an easier and cheaper shaping of the reflector to produce curved surfaces, and their continuous mode industrial elaboration allows the production of larger surfaces. Moreover, the involved materials lead to the elimination of possible breakage and increase resistance against impact and thermal shocks.

Usually all those materials are used to concentrate the radiative energy coming from the sun and they are consequently chosen for their high reflectivity over the whole solar spectrum (0.3 to 2.5 µm) and their good mechanical resistance over the time. The present study is focused on their spectral behavior within the infrared range (2 to 20 µm) and especially over the spectral range (8 to 14 µm) called the atmospheric window through which most of the terrestrial IR radiations leave the earth system.

Squares of 25 mm in side of each material were sampled from larger plates and were directly used without specific cleaning procedure to perform reflectivity measurements.

2.2 Spectral emissivity measurements

According to the energy conservation law and the first Kirchhoff's law, the spectral emittance ε_λ is related to the spectral reflectance ρ_λ and the spectral transmittance τ_λ by the following relation:

$$\varepsilon_\lambda = 1 - \rho_\lambda - \tau_\lambda \quad (1)$$

All the investigated materials have been checked to be opaque ($\tau_\lambda = 0$) within the spectral range of experimentation. Then, only one parameter is needed to describe their spectral emissivity and **Eq.1** is reduced to:

$$\varepsilon_\lambda = 1 - \rho_\lambda \quad (2)$$

Consequently to characterize the spectral emissivity of the studied samples, their spectral reflectivity was measured.

Using the experimentally obtained emissivity spectra, the spectral radiance of each sample was calculated as follows:

$$L_\lambda(T) = \varepsilon_\lambda . L_\lambda^0(T) \quad (3)$$

where $L_\lambda^0(T)$ is the spectral radiance of the blackbody which is given by Planck's law:

$$L_\lambda^0(T) = \frac{2hc^2}{\lambda^5} \frac{1}{e^{\frac{hc}{\lambda kT}} - 1} \quad (4)$$

with λ the wavelength, T the temperature and c the speed of propagation of light in vacuum, h and k are the Planck and the Boltzmann constants respectively.

By integrating the spectral radiance through the whole spectral range, we obtain the total radiance:

$$L(T) = \int_0^\infty L_\lambda(T) \quad (5)$$

Finally, making the hypothesis that the materials behave as Lambertian radiators, the radiative flux density is given by the following relation :

$$M(T) = \pi . L(T) \quad (6)$$

2.3 Experimental equipment

The reflectivity spectra at room temperature (20°C) were obtained on a FT-IR Bruker Vertex 70 spectrometer using a Globar as IR source and a Ge/KBr beam splitter. The measurements were made with an instrumental resolution of 4 cm^{-1}. Only the relevant data between 625 cm^{-1} and 1666 cm^{-1}(16 to 6 µm) corresponding roughly to the atmospheric window spectral range are reported in **Fig. 7-9**.

For specular surfaces, the normal spectral emissivity is obtainedvia the near normal specular spectral reflectivity. On the contrary, for diffuse samples, radiation reflected in other direction than specular has also to be considered. In this case, the normal emissivity is obtained via the near-normal hemispherical (or diffuse) spectral reflectivity using an integrating sphere that allows collecting radiation reflected in all directions [34].

The specular reflectivity spectra (ρ_{spec}) at an angle close to the normal (around 10°) were obtained between 350 cm^{-1} and 7500 cm^{-1} (28.6 to 1.33 µm) using a VW absolute reflectivity accessory (Bruker) and a DTGS detector.

The diffuse reflectivity spectra (ρ_{diff}) were measured between 500 cm^{-1} and 5500 cm^{-1} (20 to 1.82 µm) using an integrating sphere (Labsphere Inc.) fitted to the Bruker Vertex 70 with a MCT (Mercury Cadmium Telluride) detector (Infra Red Associates Inc.). The reflectivity is obtained by comparison of the radiation reflected from the sample to that reflected by a diffuse coating reference reflecting ~96% of the incident radiation (2 inch Gold reference – Sphere Optics). Subsequently, we will name ε_{spec} the emissivity obtained via specular reflectivity ($\varepsilon_{spec} = 1 - \rho_{spec}$) and ε_{diff} the emissivity obtained via the diffuse reflectivity ($\varepsilon_{diff} = 1 - \rho_{diff}$). The experimental set-up and these two measurement configurations are presented in **Fig. 6**.

In order to study the dependence of the emissivity with temperature, measurements have been carried out on another experimental set up, a FT-IR Nicolet 6700 spectrometer coupled to a Surface Optics SOC 100 reflectometer. The measurement principle is the same but the sample can be heated up.

3. Results and discussion

The so-called greenhouse effect of the earth/atmosphere system is partly function of the ability of the earth to transfer its infra-red (IR) radiations to space through the atmosphere layer. Depending upon the atmosphere composition and thickness, the earth IR radiations are shared between a fraction absorbed by the contributing gas and a fraction effectively discharged to space. As the exact composition of the atmosphere depends highly on the location and date, only a rough scheme as in **Fig. 4** can be given for description.

As shown in **Fig. 4**, the atmosphere is mainly and partly transparent to IR radiation between 8-14 µm, a domain currently called "atmospheric window" through which about 40% of IR radiations are transmitted. This is first mainly due to the fact that the water vapor of the atmosphere offers an IR partial transmission window between 8 and 20 µm. Then, the heat absorption peak of carbon dioxide ranging between 12 and 18 µm, restricts drastically this transmission window mainly from 8 to 14 µm. Less significantly, the ozone fraction absorbs also a part of the IR radiations around 9 and 14.5 µm. As their absorption peaks are situated in other range of wavelength, methane and nitrous oxide have no effect on the atmospheric window width.

According to the above information, the assessment of the radiative potential of the studied materials for our application has to be done through the so-called atmospheric window and by a spectral characterization. The corresponding cooling effect will be consequently estimated by the integration of the net spectral difference between the emitted IR radiations and the atmospheric transparency through the whole wavelength of the atmospheric window.

3.1 Spectral emissivity of the investigated materials

Since the atmosphere transparence is spectrally dependent, the spectral characterization of CSP reflective surfaces has been considered. We present respectively in **Fig. 7a** and**Fig. 7b**, the normal spectral emissivity of investigated materials over the spectral range 6-16 µm (1667-625 cm^{-1}) measured via the specular (ε_{spec}) and the diffuse reflectivity (ε_{diff}). According to their applications, CSP reflective surfaces are highly specular. Thus both figures are very similar since the difference is only due to the diffuse part of reflected rays estimated to be below 2.3% of the total spectral emissivity.

From a qualitative aspect, the glass mirror (GM) has a rather uniform behavior all over the inspected spectral range 6-16 µm (1667-625 cm^{-1}). Nevertheless, it presents a band of absorption between 8-12.2 µm (1250-820 cm^{-1}) with a peak at 9.5 µm (1053 cm^{-1}) due to the vibration of SiO_4 tetrahedral contained in the glass [35]. Concerning innovative surfaces, we distinguish the reflective film of silver mirror (RFSM) which has a relative uniform reflectivity value over the atmospheric window, as compared to the two aluminum mirrors (AM 1 and AM 2) which present more pronounced fluctuations. This difference is mainly due to their different respective multilayer coating composition and thickness, as previously mentioned. Nevertheless, we can still identify a common absorption band between AM 1 and AM 2 at 11.0 µm (910 cm^{-1}) corresponding to CH bending type vibrational mode. Other absorption bands over the atmospheric window for these two surfaces are presumably other vibrational modes of this same chemical bond.

In order to compare them, we report in **Table 2** only their normal spectral emissivity (ε_{spec}) mean values over the atmospheric window, since we have seen previously in **Fig. 7a** and **Fig. 7b** that the normal spectral emissivity measured via the specular (ε_{spec}) and the diffuse reflectivity (ε_{diff}) are very similar (less than 2% of difference). Thus, this fact demonstrate the specularity of investigated materials. Furthermore, we specify the respective standard deviation (SD) of each means values togive an idea of the variability of the normal spectral emissivity over the atmospheric window. It appears that all investigated materials have a good ability to emit infrared radiation over the atmospheric window. While RFSM mirror present the highest mean spectral emissivity around 0.95 within the atmospheric window, conventional materials still have a high potential with 0.85 for the GM mirror. The two aluminum mirror AM 1 and AM 2 have similar performances around 0.75 of mean spectral emissivity.

Moreover, as the investigated CSP reflective surfaces will be heated during the intended application, the relative temperature deviation of the spectral emissivity had to be considered.

This factor has been evaluated comparing the spectral emissivity characterization of the AM 2 mirror sample at different surface temperature considering the reference taken at 20°C as the ambient temperature.

In **Fig. 8** the relative spectral emissivity temperature deviation over the spectral range of 7-15 µm (1429-667 cm^{-1}) has been plotted from 20°C (taken as reference) to 70°C corresponding to the operating temperature range of the concerned application. As a result, the relative spectral emissivity deviation with the temperature, ranges between -4% and 7% with an average value around 0.3%. Consequently, the spectral emissivity of the investigated materials will be further assumed to be temperature independent.

3.2 Aging and fouling effects on the glass mirror total spectral emissivity

The deposition of organic and mineral matters on the CSP reflective surfaces are usually avoided to maintain the optical efficiency of the solar field but remains a real constrain for outdoors equipments maintained for more than 20 years. Even if regular washings using demineralized water are currently operated on those surfaces in industrial plants, the effect of such fouling on the considered surface characteristics have to be taken into account. According to the fact that the radiative properties of the surface depends strongly on the nature of the very first superficial layer of matter, the effect of dirt deposit on the IR emissivity should be considered. This issue has been assessed by the comparative characterization of raw conventional GM CSP mirrors taken at the CSP pilot plant of Themis after more than 20 years of outdoors exposition and different levels of dirt deposition. The variation of the normal spectral emissivity (ε_{diff}) with respect to the wavelength is illustrated in **Fig.9** for all experimented samples. The obtained results highlight a common general trend imposed by the SiO_4 peak depletion at 9.4 µm advantageously balanced by the deposits. For the dirtiest GM sample, the minimum value of the normal spectral emissivity is 14% higher than for the raw but clean GM. Consequently, while the dirt deposition on the CSP reflective surfaces is disadvantageous for regular solar applications, it is proved to be advantageous for the corresponding IR radiative cooling technique. This fact will be considered in the future studies by using clean surfaces while subsequent industrial applications will take advantage of a potential enhancement of the radiative properties with time.

3.3 Estimation of the emitted and transmitted radiative flux density

In order to estimate the radiative heat transfer contribution in the cooling process of thermodynamic cycle trough the solar field, the radiative flux density range emitted and transmitted have been determined.

So firstly, according to the normal spectral emissivity (ε_{diff}) presented in **Fig. 7b** and using **Eq. 3** for the spectral radiance of the blackbody, the spectral radiance emitted from the investigated materials over the spectral range 2-20 µm (5000-500 cm^{-1}) is presented in **Fig.**

10a and **Fig. 10b** at 20°C and 60°C respectively, which correspond to the minimum/maximum operating temperature of the concerned application.

Secondly, according to the atmospheric window represented in **Fig. 4** and the spectral radiance emitted from the investigated materials presented in **Fig. 10a** and **Fig. 10b**, the spectral radiance discharged into the extra atmospheric space at 3K over the spectral range 6-16 µm (1667-625 cm^{-1}) is presented in **Fig. 11a** and **Fig. 11b** at the two temperature levels, 20°C and 60°C respectively.

Finally, according to **Eq. 5** and **Eq. 6**, the minimum (at 20°C) and the maximum (at 60°C) thermal radiative flux density emitted by the investigated materials and discharged into the extra atmospheric space are gathered in **Table 3** for comparison. A percentage of their respective performances is also given for comparison to the blackbody reference (noticed $\%_{BB}$ in italic). The ratio between the emitted flux density and the transmitted flux density correspond to the atmospheric attenuation.

As highlighted in **Table 3**, in terms of raw emitted flux at 20 and 60°C, the most efficient surface seems to be the conventional CSP-GM surface followed very closely by the innovative RFSM while AM 1 and AM 2 surfaces present similar and clearly lower performances.

If we take into account within the atmospheric window, the ability of the atmosphere to allow the IR radiation to leave the earth system for each wavelength, the comparison between the different materials leads to other conclusions. The net flux transmitted to the extra atmospheric space shows that the innovative film RFSM offers the best performances at both temperatures closely followed by the conventional CSP GM while the two AM 1 and AM 2 still present similar and lower performances.

This spectral analysis of the net discharged flux illustrates the antagonistic or balanced effects between the surface behavior and the atmosphere. As instance, the disadvantageous (in terms of IR emission) SiO_4 tetrahedral peak of the CSP GM glass mirror, is mainly balanced by absorption peak of the O_3 contained in the atmosphere.

According to those estimations, the radiative contribution to the expected net cooling effect ranges from 18 to 24% of the CSP plant cooling needs. Combined with the convective heat exchanges, this highlights the significant subcooling potential of the radiative transfer for the application.

4. Conclusion

In the context of potential conflict of use between power production and the so strategic water resource, critical needs in alternative and efficient dry cooling technologies have been highlighted as a key challenge for the CSP market growing. As a potential approach, the solar field of the CSP plant, offering huge available surfaces, has been already proposed as macro heat exchangers. Thanks to the advantageous atmospheric conditions in the arid areas, this

cooling effect is shared between the conventional convective heat transfer with the surrounding air and the less currently used radiative effect with the extra atmospheric space at 3K. While the convective part can be calculated, the estimation of the radiative one suffers of lack in IR emissivity assessments of the corresponding surfaces. The aim of the present study is to overcome this shortcoming not only in the case of conventional CSP glass mirrors but considering also innovative reflective surfaces potentially available for next solar fields generations.

According to the fact that the transparency of the atmospheric window to the IR radiation is strongly dependent to the wavelength, the conventional and innovating materials have been characterized in terms of spectral infrared emissivity. RFSM aluminum film appears to be the most efficient one with a mean spectral emissivity around 95%, while conventional glass mirrors GM performances are around 86%. Moreover, within the spectral range of the atmospheric window 8-14 µm, the emissivity of the aluminum film presents less variations than the glass mirror with a respective standard deviation of 3 and 7.8 respectively. Nevertheless, the particular SiO_4 tetrahedral peak responsible to the local decrease in emissivity of the GM at 9.5 mm is mainly balanced by the corresponding adsorption peak of the ozone present in the atmosphere. Then, the net cooling effect through the atmospheric window is still favorable to the RFSM which present the best performances, followed closely by the GM. Comparatively, AM 1 and AM 2 aluminum mirrors present similar and lower performances for the cooling application.

Moreover, the fouling effect of those outdoor surfaces on the IR emissivity have been also studied, leading to an increase in the expected performances. Then, the characterization of the raw and clean reflective surfaces can be directly used to design such cooling systems.

The results illustrate the fact that the solar field reflective surfaces can be used not only as solar concentrators but also as efficient cooling surfaces. Consequently, they offer the major advantage to be used not only nightly but 24h/day. The radiative contribution to the whole heat transfer offer the advantage to sub-cool the system below the ambient temperature. The particular performances of the reflective films associated to their low weight and cost highlight their high potential for next generation of CSP solar fields.

Next steps in the study will focus on the corresponding cooling performances obtained when using comparatively the surfaces on outdoor prototypes under different weather conditions.

Acknowledgements

The authors acknowledge the financial supports of the French government through the ANR within the frame of the DryRSP project. This work was supported by the French "Investments for the Future" program managed by the National Agency for Research under contract ANR-10-LABX-22-01 (Labex SOLSTICE). The authors thank Aurélien Canizares, Lionel Cosson and Jean-Marie Mancaux for their technical support.

References

[1] World Energy Council, Deciding the Future: Energy Policy Scenarios to 2050 (2007).

[2] IEA, Technology Roadmap: Concentrating Solar Power, IEA Report (2010).

[3] C. Richter, Cooling of CSP plants in solar power and chemical energy systems,International Energy Agency SolarPaces Annual Report (2011)2.1-2.5.

[4] J.A. Gary, K. Ho Clifford, T.R. Mancini, G.J. Kolb, N.P. Siegel, B.D. Iverson, Development of a power tower technology roadmap for DOE,SolarPaces (2010).

[5] J.J. Burkhardt, G.A. Heath, C.S. Turchi, Life cycle assessment of a parabolic trough concentrating solar power plant and the impacts of key design alternatives,Env. Sci.& Tech.45(2011)2457–2464.

[6] D. Laing, W.D. Steinmann, R. Tamme, C. Richter, Solid media thermal storage for parabolic trough power plants,Sol. Energy80(2006)1283–1289.http://dx.doi.org/10.1016/j.solener.2006.06.003

[7] X. Py, N. Calvet, R. Olives, A. Meffre, P. Echegut, C. Bessada, E. Veron,S. Ory,Recycled material for sensible heat based thermal energy storage to be used in concentrated solar thermal power plants,J. Sol. Energy Eng.133 (3) (2011).

[8] F. Delaleux, Enhancement of energy processes performances by hybridization of solar and geothermal energies,PhD thesisof the University of Perpignan (2011).

[9] D. Rochier, V. Goetz, X.Py, R. Olives, G. Flamant, Improved element for processing solar radiation, and a sun tracker and a solar farm equipped with such an element,Patent WO2014091172A3(2013).

[10] H. Espargilliere, Innovative approach for dry cooling of thermodynamic Rankine solar power plants,Energy Procedia(2014)SolarPaces.

[11] M. Zeyghami, F. Khalili, Performance improvement of dry cooled advanced concentrating solar power plants using daytime radiative cooling, Energy Conv.&Manag.106 (2015) 10-20.http://dx.doi.org/10.1016/j.enconman.2015.09.016

[12] A. Dyreson, F. Miller, Night sky cooling for concentrating solar power plants,Appl. Energy180(2016) 276-286.http://dx.doi.org/10.1016/j.apenergy.2016.07.118

[13] R. Pitz-Paal, J. Dersch, B. Milow,European Concentrated Solar Thermal Road-Mapping,European project ECOSTAR SES6-CT-2003-502578 (2004).

[14] M. Lemouari, M. Boumaza, I.M.Mujtaba, Thermal performances investigation of a wet cooling tower,Appl. Therm. Eng. 27 (2007)902-909.http://dx.doi.org/10.1016/j.applthermaleng.2006.08.014

[15] J. Budik, Heller indirect dry cooling system: Dry cooling solution from the polar circle to hot deserts, GEA Heat exchangers, Russia Power (2013), available at http://pennwell.sds06.websds.net/2013/moscow/rp-hvr/slideshows/T2S7O1-slides-en.pdf (accessed 28.06.2017).

[16] O.K. Sadaghiyani, S. Khalilaria, I. Mirzaee, Energic, exergic, exergo-economic investigation and optimization of Auxiliary Cooling System (ACS) equipped with Compression Refrigerating System (CRS), Case Stud. Therm. Eng. (2017), DOI: http://dx.doi.org/10.1016/j.csite.2016.12.004

[17] J.G.Bustamante, A.S.Rattner, S.Garimella, Achieving near-water-cooled power plant performance with air-cooled condensers,Appl. Therm. Eng. 105 (2016)362-371.http://dx.doi.org/10.1016/j.applthermaleng.2015.05.065

[18] A. Poullikkas, I. Hadjipaschalis, G. Kourtis, A comparative overview of wet and dry cooling systems for Rankine cycle based CSP plants,Trends in Heat & Mass Transf.13 (2013).

[19] P. Palenzuela, G. Zaragoza, D.C. Alarcon-Padilla, E. Guillén, M. Ibarra, J. Blanco, Assessment of different configurations for combined parabolic-trough (PT) solar power and desalination plants in arid regions, Energy 36 (2011)4950–4958.http://dx.doi.org/10.1016/j.energy.2011.05.039

[20] P. Palenzuela, G. Zaragoza, D.C. Alarcon-Padilla, J. Blanco, Evaluation of cooling technologies of concentrated solar power plants and their combination with desalination in the mediterranean area,Appl. Therm. Eng. 50 (2013)1514-1521.http://dx.doi.org/10.1016/j.applthermaleng.2011.11.005

[21] X. Zhou, J. Yang, B. Xiao, G. Hou, Experimental study of temperature field in a solar chimney power setup,Appl. Therm. Eng. 27(2007)2044-2050.http://dx.doi.org/10.1016/j.applthermaleng.2006.12.007

[22] X. Zhou, J. Yang, B. Xiao, G. Hou, F. Xing, Analysis of chimney height for solar chimney power plant,Appl. Therm. Eng. 29 (2009)178-185.http://dx.doi.org/10.1016/j.applthermaleng.2008.02.014

[23] D. Bonnelle, F. Siros, C. Philiberts, Concentrating solar parks with tall chimneys dry cooling,Proceeding of the SolarPacesConference, Perpignan (2010).

[24] F. Trombe, "Devices for lowering the temperature of a body by heat radiation therefrom." USPTO, Patent US3310102A (1967).

[25] B. Orel, MK. Gunde, A. Krainer, Radiative cooling efficiency of white pigmented paints,Sol. Energy50(1993)477–482.http://dx.doi.org/10.1016/0038-092X(93)90108-Z.

[26] H.S Bagiorgas, G. Mihalakakou, Experimental and theoretical investigation of a nocturnal radiator for space cooling,Renew. Energy33(2008)1220–1227. http://dx.doi.org/10.1016/0038-092X(93)90108-Z.

[27] S.N. Bathgate, S.G. Bosi, A robust convection cover material for selective radiative cooling applications,Sol. Energy Mater.& Sol. Cells95 (2011)2778–2785.http://dx.doi.org/10.1016/j.solmat.2011.05.027

[28] T.M.J. Nilsson, G.A. Niklasson, Radiative cooling during the day: simulations and experiments on pigmented polyethylene cover foils,Sol. Energy Mater.&Sol. Cells, 37(1995)93–118.doi:10.1016/0927-0248(94)00200-2

[29] K. Dobson, G. Hodes, Y. Mastai, Thin semiconductor films for radiative cooling applications,Sol. Energy Mater.&Sol. Cells80(2003)283–296.http://dx.doi.org/10.1016/j.solmat.2003.06.007

[30] E. Erell, Y. Etzion, Radiative cooling of buildings with flat-plate solar collectors,Build.& Environ.35 (2000)297–305.http://dx.doi.org/10.1016/S0360-1323(99)00019-0

[31] M. Muselli, D. Beysens, J. Marcillat, I. Milimouk, T. Nilsson,A. Louche, Dew water collector for potable water in Ajaccio (Corsica Island, France),Atmos.Res.64 (2002)297–312.http://dx.doi.org/10.1016/S0169-8095(02)00100-X

[32] D. Beysens, I. Milimouk, V. Nikolayev, M. Muselli,J. Marcillat, Using radiative cooling to condense atmospheric vapor: a study to improve water yield,J.Hydrol.276(2003)1–11.http://dx.doi.org/10.1016/S0022-1694(03)00025-8

[33] CSP World, The Microsol project inaugurates its first CSP demonstrator in France, http://www.csp-world.com/news/20131125/001261/microsol-project-inaugurates-its-first-csp-demonstrator-france, 2013 (accessed 07.10.16).

[34] A. Dupleix, D. De Sousa Meneses, M. Hughes, R. Marchal, Mid-infrared absorption properties of green wood, Wood Sci. Technol 47 (2013) 1231–1241. http://dx.doi.org/10.1007/s00226-013-0572-5

[35] K.M.Davis,M. Tomozawa, An infrared spectroscopic study of water-related species in silica glasses,J.Non-Cryst. Solids201 (1996)177–198.http://dx.doi.org/10.1016/0022-3093(95)00631-1

Figures and tables

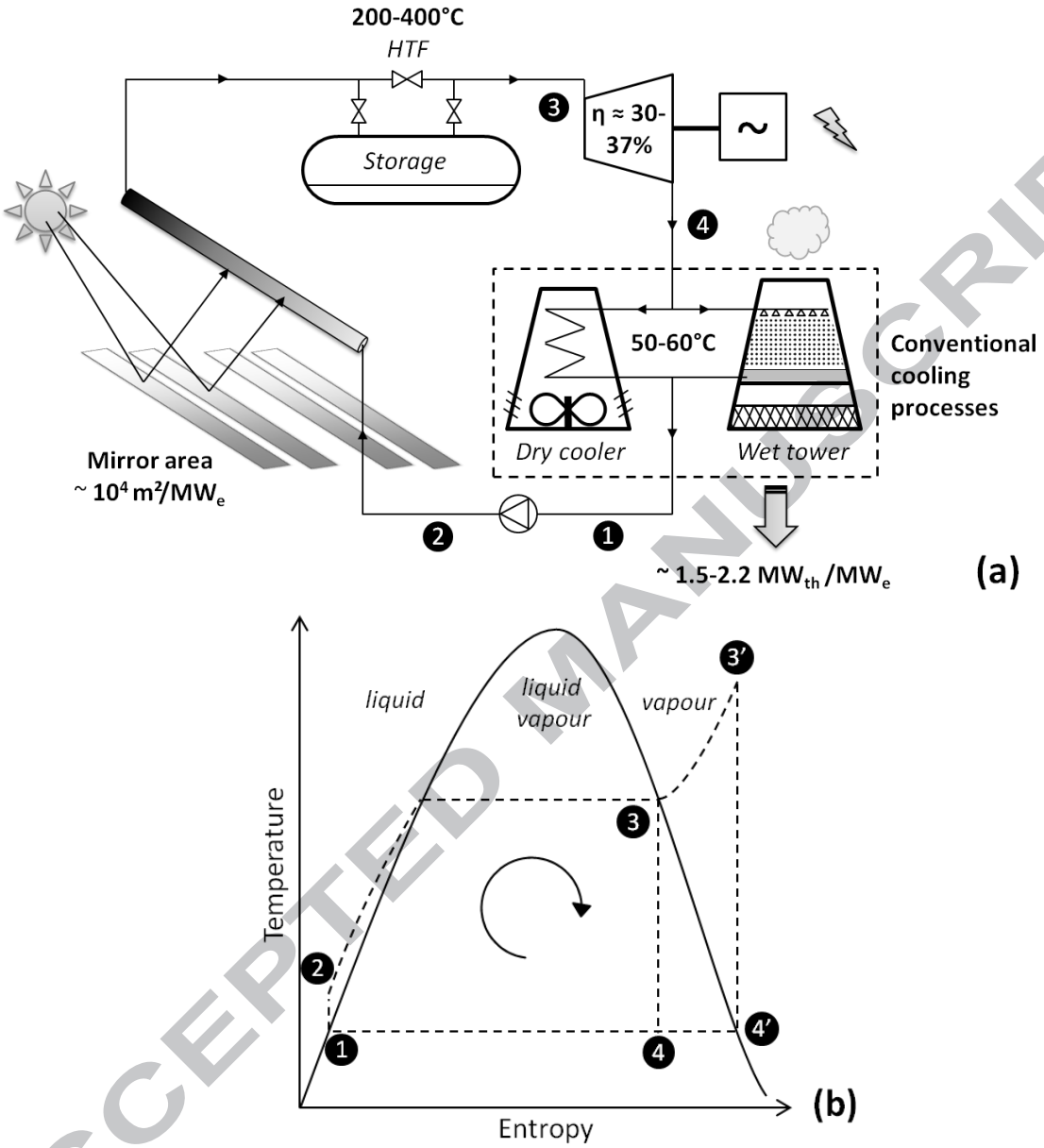

Figure 1 : Diagram of linear Fresnel CSP plant with conventional cooling system (a) and its corresponding steam Rankine cycle (b).

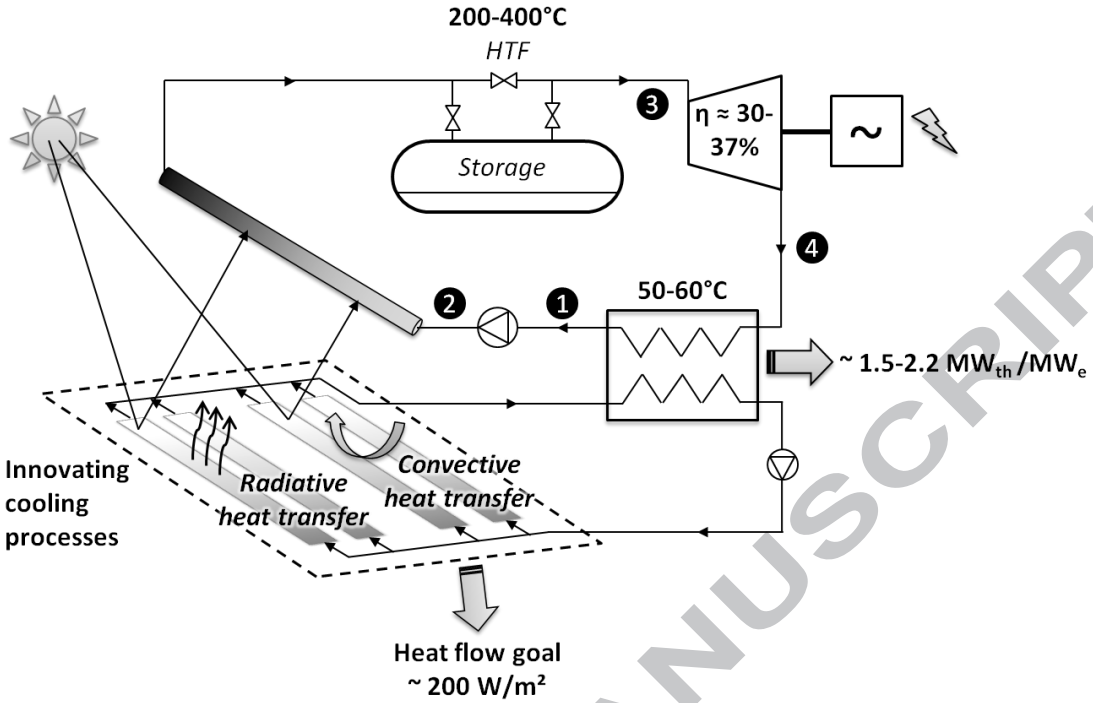

Figure 2 : Diagram of linear Fresnel CSP plant with innovative cooling system.

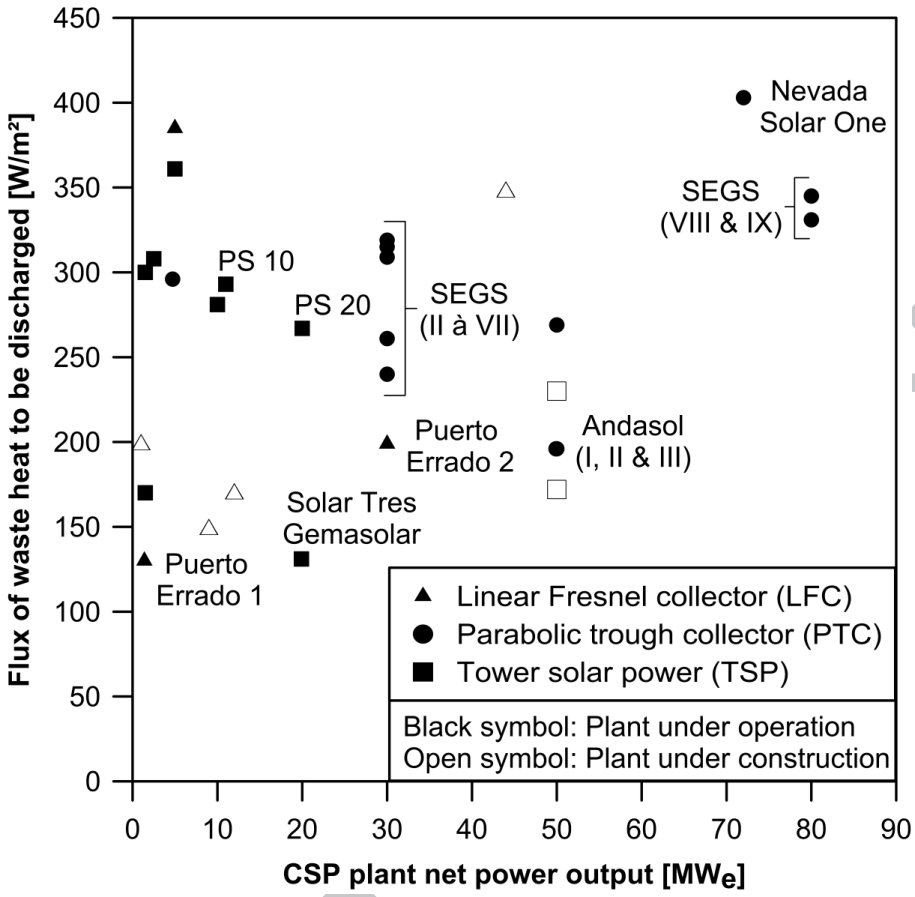

Figure 3 : Expected flux of waste heat to be discharged as a function of the CSP plant net power output.

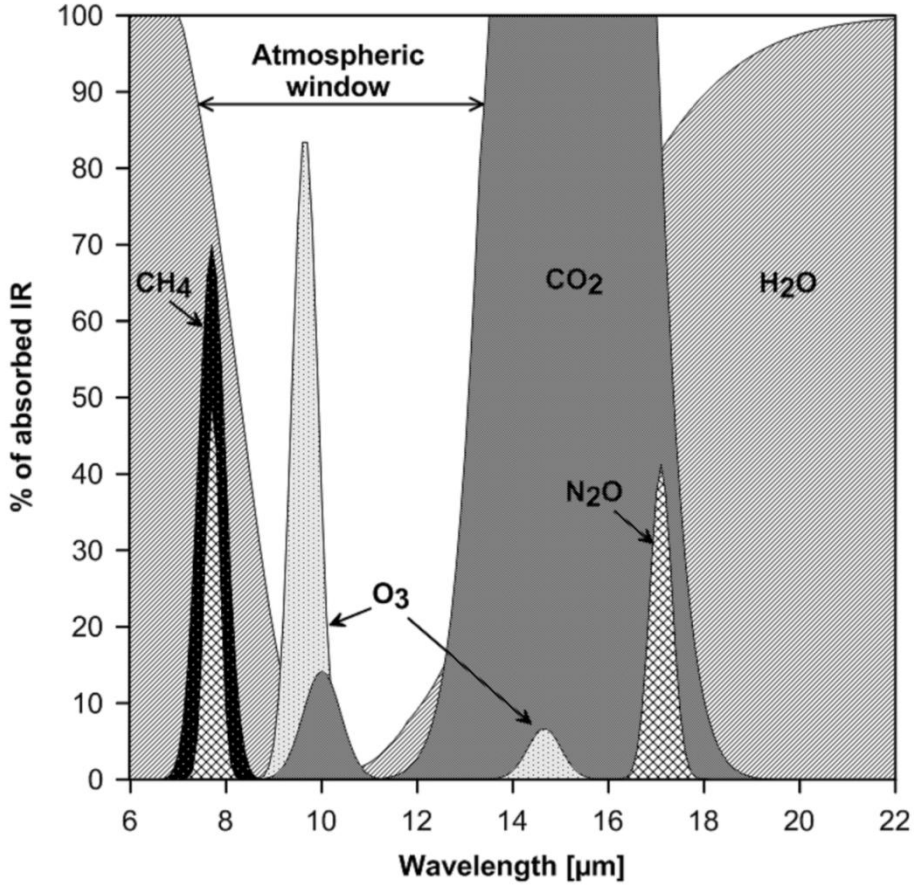

Figure 4 : Infrared radiations absorbed by greenhouse gases.

(a) (b)

Figure 5 : Conventional Linear Fresnel mirror on its support and dedicated rotational axis(a), flat Roll-bond heat exchanger on its channeled side (the other side is flat and supports the mirror)(b).

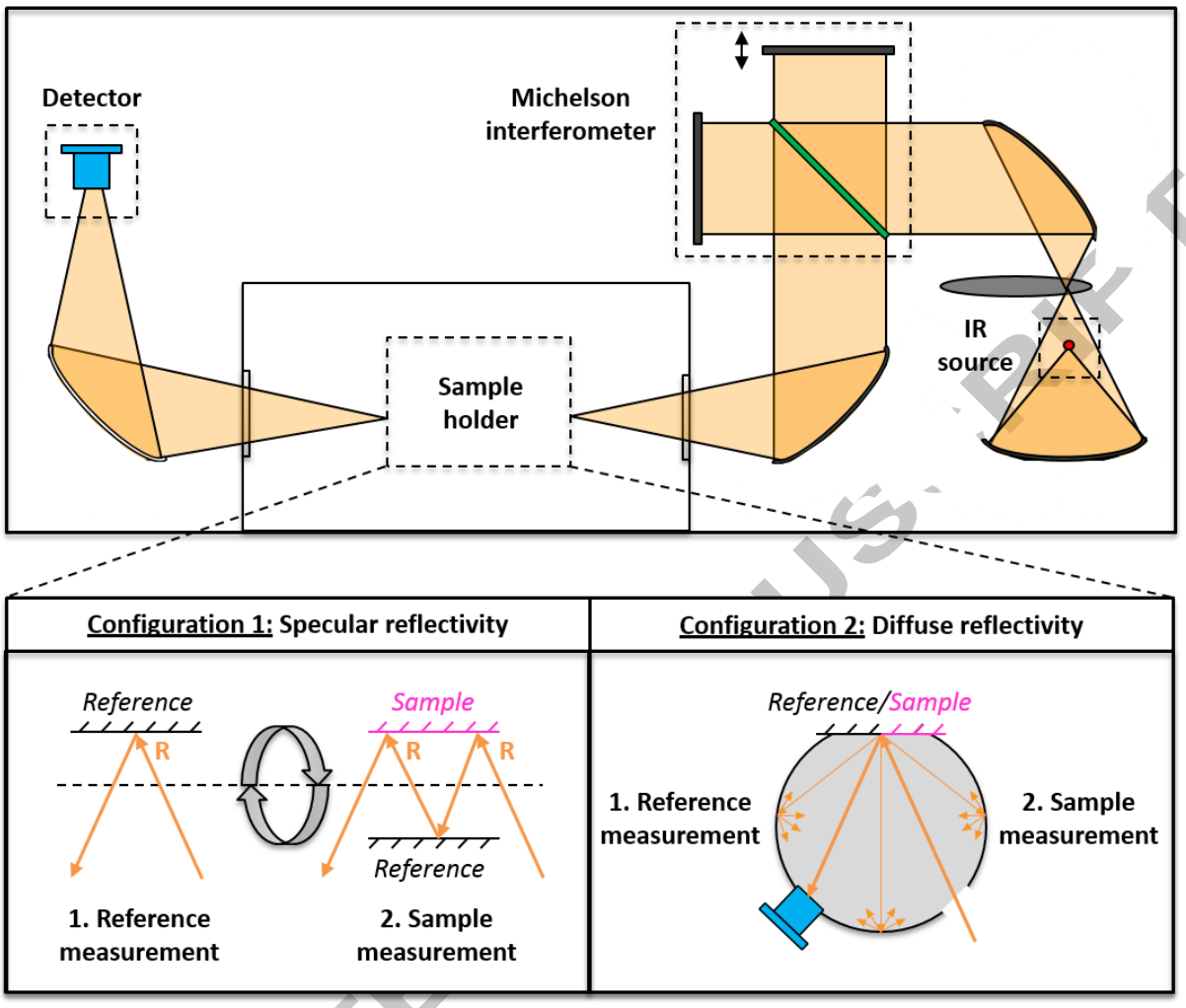

Figure 6 : Schematic representation of the FT-IR Bruker Vertex 70 spectrometer with specular (1) and diffuse (2) reflectivity measurement configuration.

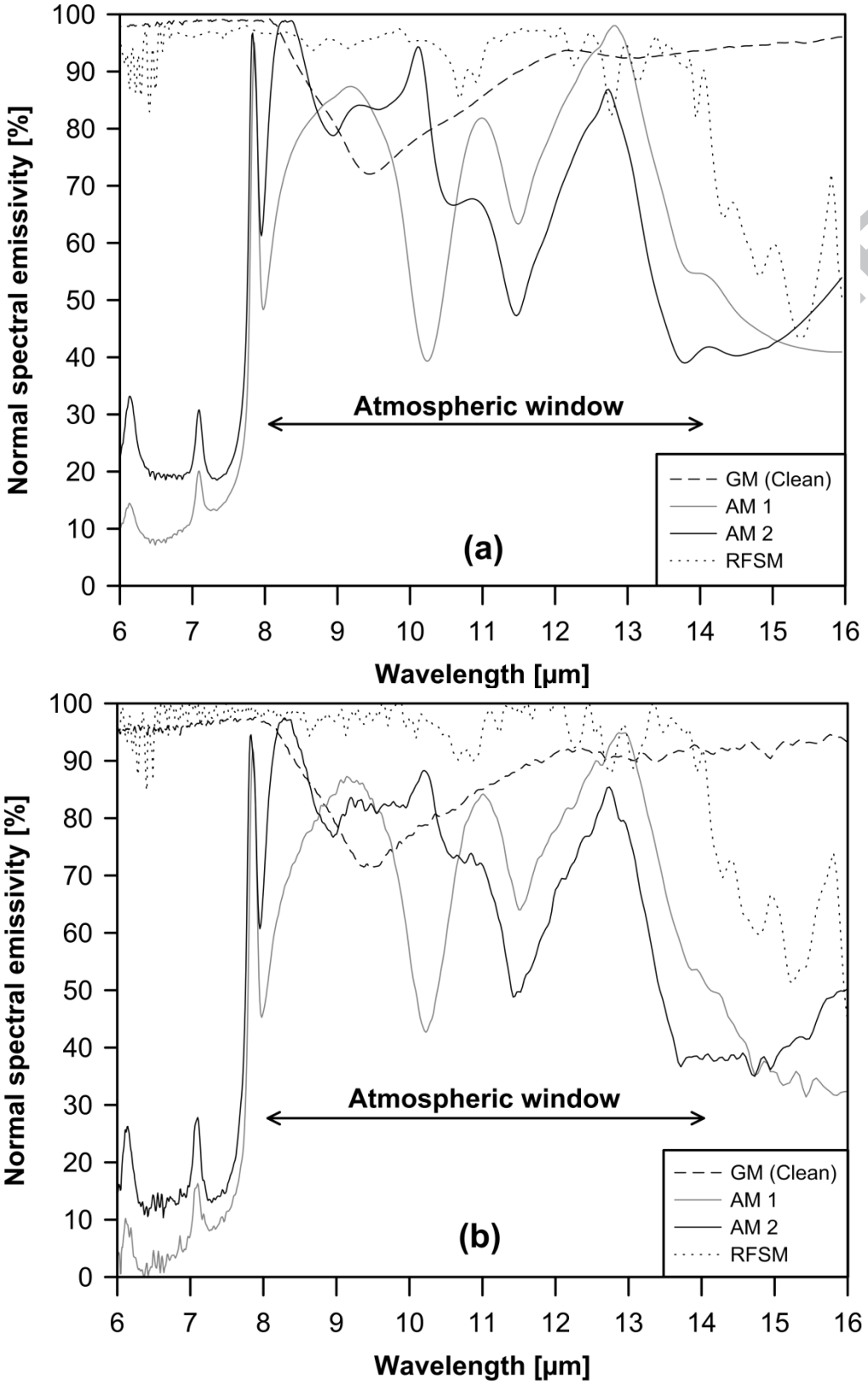

Figure 7 : Normal spectral emissivity obtained via the specular reflectivity (ε_{spec})(a) and via the diffuse reflectivity (ε_{diff}) (b) of CSP reflective materials.

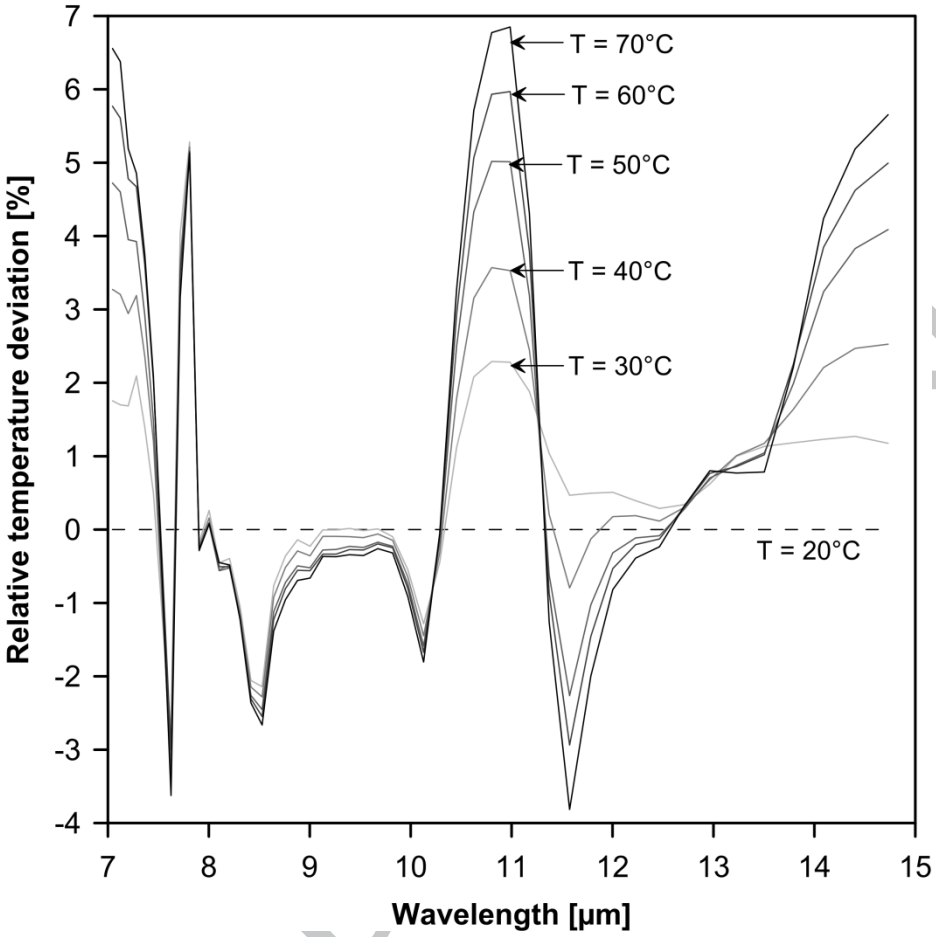

Figure 8 : Relative temperature deviation of the AM 2 mirror normal spectral emissivity.

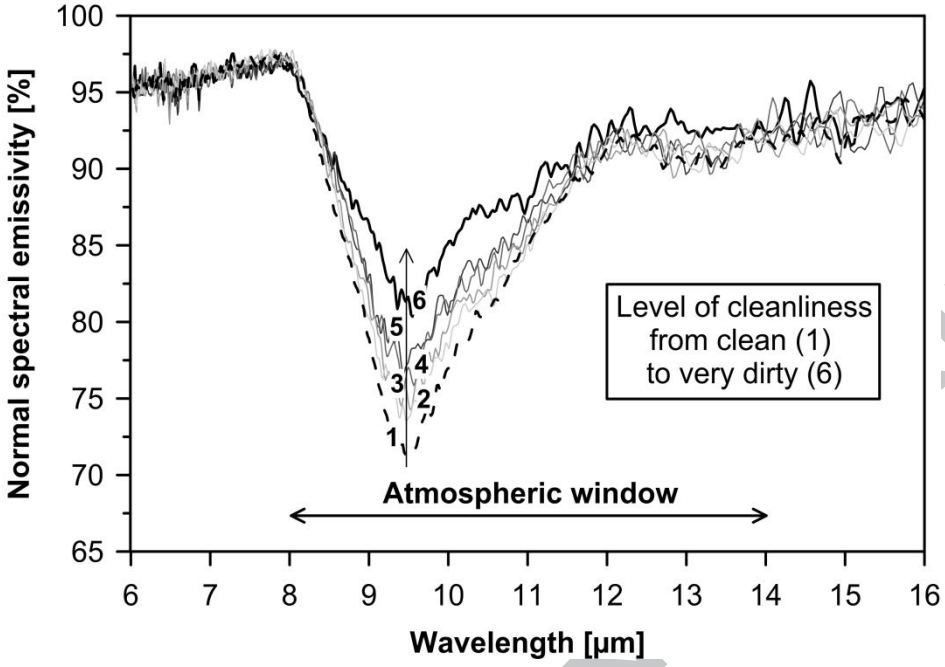

Figure 9 : Impact of dirt accumulation on GM normal spectral emissivity (ε_{diff}).

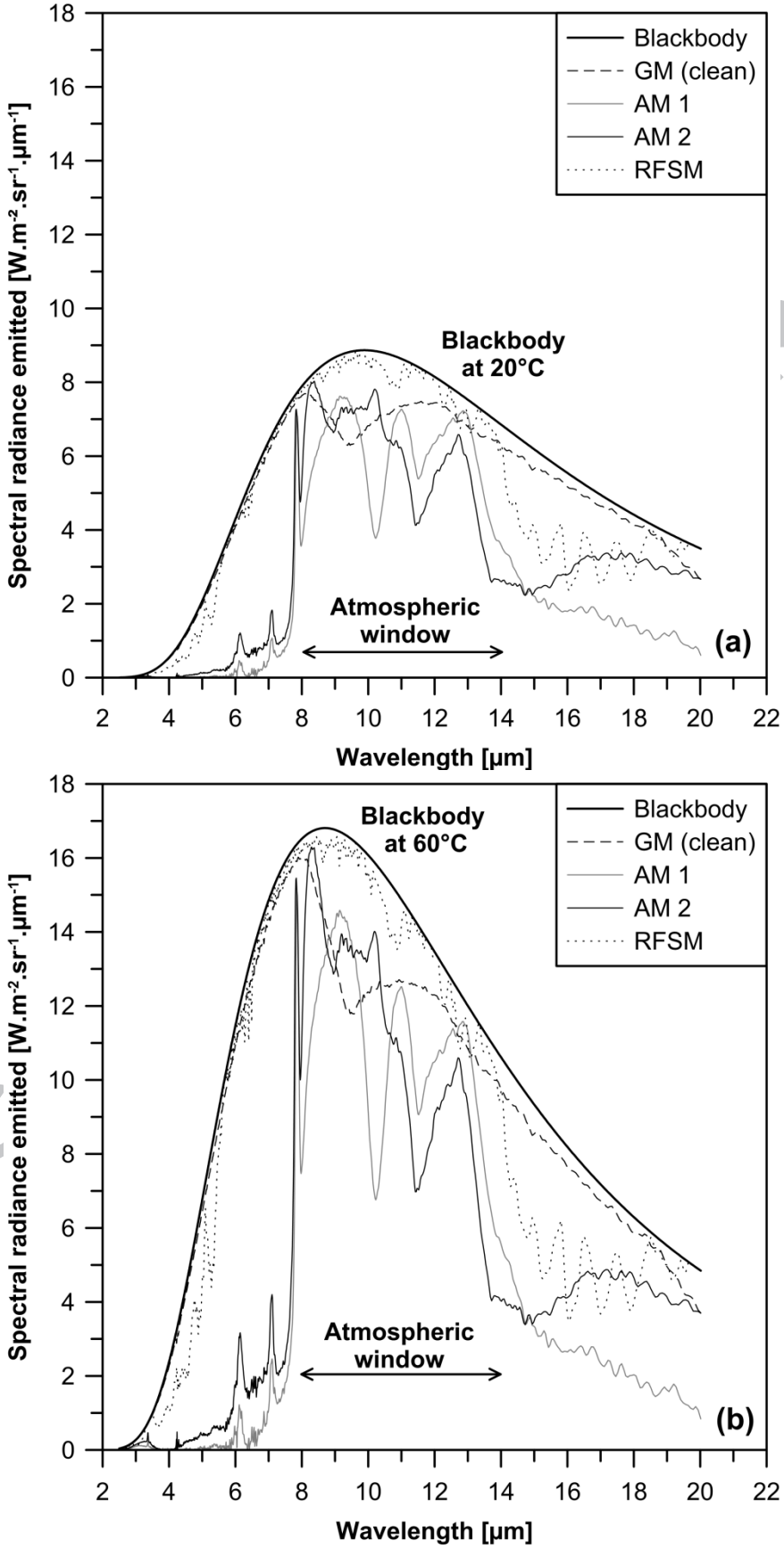

Figure 10 : Spectral radiance emitted of investigated materials at 20°C (a) and 60°C (b).

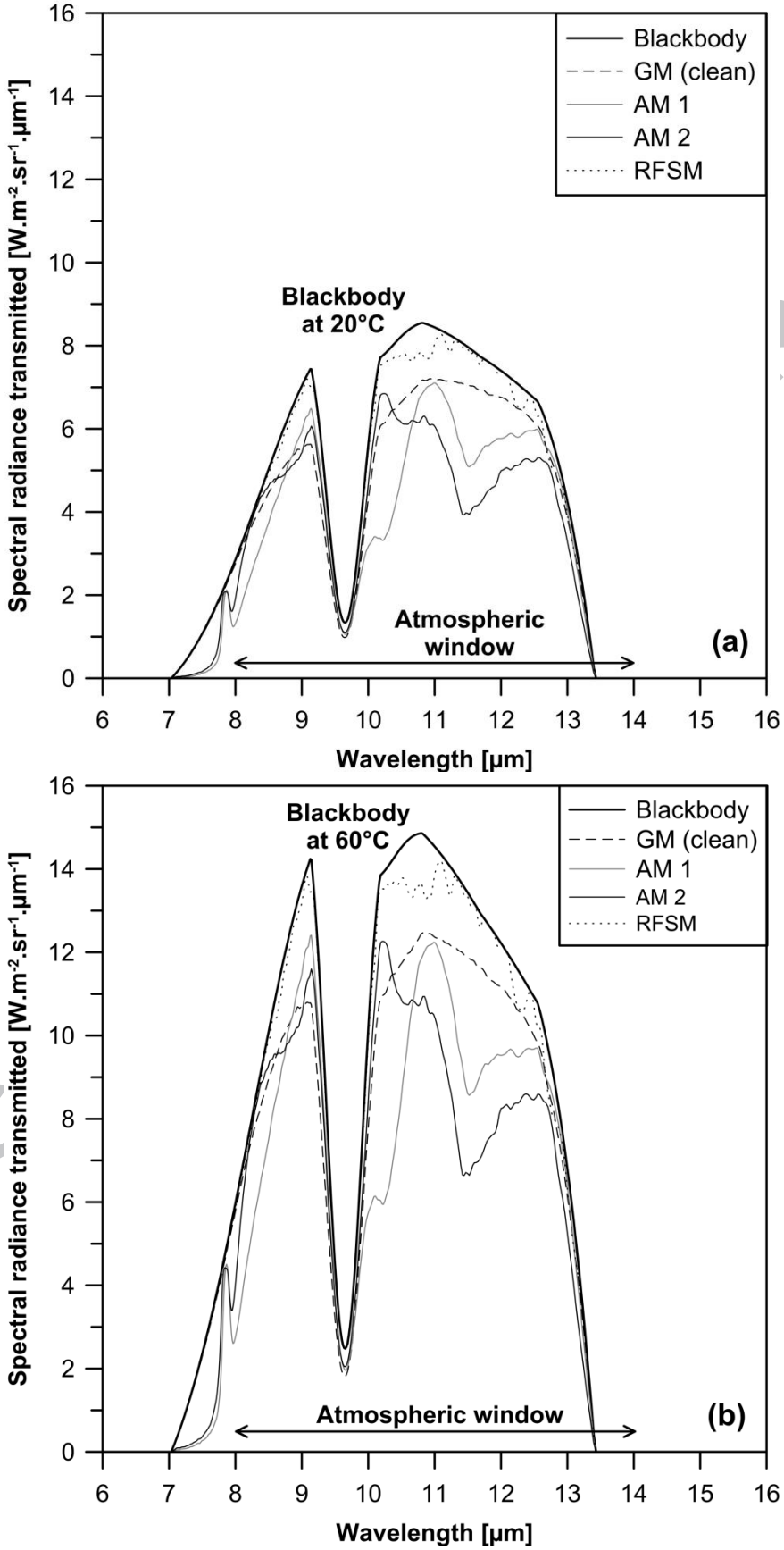

Figure 11 : Spectral radiance transmitted of investigated materials at 20°C (a) and 60°C (b).

Technology	Project name *(Start year)*	Electrical poweroutput [MW]	Waste heatpower output [MW]	Mirror area [m²]	Storage system	Storage capacity [h]	Expected discharge flux [W/m²]
Linear Fresnel concentrator (LFC)	Puerto Errado 1 *(2009)*	1.4	3	21 567	-	-	139
	Puerto Errado 2 (*2012)*	30	60	302 000	Single-tank thermocline	0.5	199
	Alba Nova 1 *(2014)*	12	24	140 000	Other	1	171
Parabolic trough concentrator (PTC)	SEGS II to VII *(1984/1988)*	30 each	60	188 000 250 500	-	-	319 240
	SEGS VIII & IX *(1989/1990)*	80 each	160	470 000	-	-	340
	Nevada Solar One *(2007)*	72	144	357 200	Single-tank thermocline	0.5	403
	Andasol I, II & III *(2008/2011)*	50 each	100	510120	2 tank indirect	7.5	196

Table 1 : Expected flux of waste heat to be discharged for different CSP plants according to their respective characteristics.

Class of material	**Type of surface**	**Normal spectral emissivity** (ε_{spec}) in [8-14 µm]
Conventional materials	CSP GM	**0.85±2%** *(0.073 SD)*
Innovating materials	AM 1	**0.74±2%** *(0.129 SD)*
	AM 2	**0.76±2%** *(0.142 SD)*
	RFSM	**0.97±2%** *(0.030 SD)*

Table 2 : Normal spectral emissivity (ε_{spec})mean value over the atmospheric window with its standard deviation (SD) of investigated materials.

Class of material	Type of surface	Flux density emitted [W/m²]* at 60°C	Flux density emitted [W/m²]* at 20°C	Flux density transmitted [W/m²] at 60°C	Flux density transmitted [W/m²] at 20°C	Atmospheric attenuation
Blackbody		**550**	**304**	**193**	**109**	-65 %
Conventional materials	CSP GM	**494** *(90 $\%_{BB}$)*	**272** *(90 $\%_{BB}$)*	**165** *(86 $\%_{BB}$)*	**94** *(86 $\%_{BB}$)*	-66 %
Innovating materials	AM 1	**264** *(48 $\%_{BB}$)*	**154** *(51 $\%_{BB}$)*	**139** *(72 $\%_{BB}$)*	**79** *(72 $\%_{BB}$)*	-48 %
	AM 2	**308** *(56 $\%_{BB}$)*	**179** *(59 $\%_{BB}$)*	**142** *(74 $\%_{BB}$)*	**80** *(73 $\%_{BB}$)*	-55 %
	RFSM	**486** *(88 $\%_{BB}$)*	**267** *(88 $\%_{BB}$)*	**185** *(96 $\%_{BB}$)*	**104** *(95% $_{BB}$)*	-62 %

* Flux emitted in the spectral range 2-20 µm (5000-500 cm^{-1}).

Table 3 : Flux density emitted and transmitted of investigated materials.

List of figures and tables

Figure 1 :Diagram of linear Fresnel CSP plant with conventional cooling system (a) and its corresponding steam Rankine cycle (b).

Figure 2 : Diagram of linear Fresnel CSP with innovative cooling system.

Figure 3 :Expected flux of waste heat to be discharged as a function of the CSP plant net power output.

Figure 4 : Infrared radiations absorbed by greenhouse gases.

Figure 5 : (a) Conventional Linear Fresnel mirror on its support and dedicated rotational axis, (b) flat Roll-bond heat exchanger on its channeled side (the other side is flat and supports the mirror).

Figure 6 : Schematic representation of the FT-IR Bruker Vertex 70 spectrometer with specular (configuration 1) and diffuse (configuration 2) reflectivity measurement arrangement.

Figure 7 : Normal spectral emissivity obtained via the specular reflectivity (ε_{spec}) (a) and via the diffuse reflectivity (ε_{diff})(b) of CSP reflective materials.

Figure 8 : Relative temperature deviation of the AM 2 mirror normal spectral emissivity.

Figure 9 : Impact of dirt accumulation on GMnormal spectral emissivity(ε_{diff}).

Figure 10 : Spectral radiance emitted of investigated materials at 20°C (a) and 60°C (b).

Figure 11 : Spectral radiance transmitted of investigated materials at 20°C (a) and 60°C (b).

Table 1 : Expected flux of waste heat to be discharged of different CSP plants according to their respective characteristics.

Table 2 :Normal spectral emissivity (ε_{spec})mean valueover the atmospheric window with its standard deviation (SD) of investigated materials.

Table 3 :Flux density emitted and transmitted of investigated materials.

Highlights

1. the spectral infrared emissivity of CSP reflectors have been characterized
2. aluminum films present higher performances than glass or aluminum mirrors
3. the fouling induced by outdoors conditions increases the IR radiative emissivity
4. the CSP solar field can be used as macro-heat-exchanger for dry cooling